Journal of Sound and Vibration 332 (2013) 3134–3147

Contents lists available at SciVerse ScienceDirect

Journal of Sound and Vibration

journal homepage: www.elsevier.com/locate/jsvi

Nonlinear stochastic controllers for power-flow-constrained vibratory energy harvesters

Ian L. Cassidy [a,*], Jeffrey T. Scruggs [b]

[a] Department of Civil & Environmental Engineering, Duke University, Durham, NC, USA
[b] Department of Civil & Environmental Engineering, University of Michigan, Ann Arbor, MI, USA

ARTICLE INFO

Article history:
Received 30 June 2012
Received in revised form
16 December 2012
Accepted 13 January 2013
Handling Editor: D.J. Wagg
Available online 19 February 2013

ABSTRACT

This study addresses the formulation of nonlinear feedback controllers for stochastically excited vibratory energy harvesters. Maximizing the average power generated from such systems requires the transducer current to be regulated using a bi-directional power electronic converter. There are many applications where the implementation of these types of converters is infeasible, due to the higher parasitic losses they must sustain. If instead the transducer current is regulated using a converter capable of single-directional power-flow, then these parasitic losses can be reduced significantly. However, the constraint on the power-flow directionality restricts the domain of feasible feedback laws. The only feasible linear feedback law imposes a static relationship between current and voltage, i.e., a static admittance. In stochastic response, the power generation performance can be enhanced significantly beyond that of the optimal static admittance, using nonlinear feedback. In this paper, a general approach to nonlinear control synthesis for power-flow-constrained energy harvesters is presented, which is analytically guaranteed to outperform the optimal static admittance in stationary stochastic response. Simulation results are presented for a single-degree-of-freedom resonant oscillator with an electromagnetic transducer, as well as for a piezoelectric bimorph cantilever beam.

1. Introduction

Over the last decade, significant research activity has been devoted to developing electromechanical systems that harvest energy from ambient mechanical vibrations. Most of the research activity has been motivated by the need to power wireless intelligence systems embedded within smart structures [1,2]. Of the several modes of transduction available for these milliwatt-scale applications, piezoelectric approaches [3,4] have received the most attention. Large-scale energy harvesting from vibrating structures has also recently been shown to be a viable source of renewable energy. The use of electromagnetic transducers has been investigated to extract power from vibrations in automotive suspensions [5], railway systems [6], wave excitations on offshore structures [7], and wind excitations on buildings [8]. The available power from such applications has been estimated at the watt- to kilowatt-scale.

Regardless of the application or scale, one of the most challenging aspects of this technology concerns the efficient extraction and transmission of power from a transducer to a storage device (e.g., supercapacitor or rechargeable battery).

* Corresponding author. Tel.: +1 919 660 5200.
E-mail address: ian.cassidy@duke.edu (I.L. Cassidy).

0022-460X/$ - see front matter © 2013 Elsevier Ltd. All rights reserved.
http://dx.doi.org/10.1016/j.jsv.2013.01.023

A considerable amount of research has focused on the use of single-directional DC/DC switching converters to regulate the power extracted by energy harvesters [9–12]. In Refs. [11,12], it was shown that operating DC/DC converters in discontinuous conduction results in an input resistance that is insensitive to the dynamics of the input and output voltages. As such, this enables the effective resistance of the converter to be designed for maximal power absorption, and then for the corresponding duty cycle to be found from this resistance. This technique effectively imposes a constant, or static, feedback law between the transducer voltage and the controlled current, as

$$i(t) = -Y_c v(t) \tag{1}$$

where $i(t)$ is the current into the transducer, $v(t)$ is the transducer voltage, and Y_c is a time-invariant feedback gain, which has units of admittance.

In Refs. [13,14], Scruggs investigated the substitution of a single-directional DC/DC converter for a fully active H-bridge converter capable of two-way power-flow. This type of converter enables unconstrained dynamic feedback control of the transducer current, i.e.

$$\hat{i}(s) = -Y(s)\hat{v}(s) \tag{2}$$

where "hats" denote Laplace-domain signals, and $Y(s)$ is the dynamic feedback law imposed by the converter. In those studies, it was shown that if the disturbance is modeled as a broadband stochastic process then the derivation of the optimal feedback control law can be found as the solution to a nonstandard linear-quadratic-Gaussian (LQG) control problem. Implementation of the optimal feedback control law $Y(s)$ requires a bi-directional converter, and a follow-up study by Cassidy et al. [15] illustrated the improvement in performance that can be achieved with the optimal $Y(s)$, as opposed to Y_c, for both piezoelectric and electromagnetic energy harvesters.

Every time a MOSFET in a power electronic converter is switched on, a small amount of energy must expended, to charge the gate capacitance. It is very difficult to recover this energy when the MOSFET is switched off again. When a MOSFET is switched in pulse-width modulation at high frequency, there is a parasitic power loss, due to this switching energy. Single-directional converters facilitate pulse-width modulation with only a single MOSFET. By contrast, an active H-bridge uses four MOSFETS, and requires two to be gated each switching cycle. The switching logic and gate drive circuitry for active H-bridges can also be more complicated. Therefore, they consume considerably more parasitic power than single-directional converters, which is the price paid for two-way power directionality. For very small power scales, this price far exceeds the benefit of bi-directional power-flow, making single-directional converters the more viable technology.

This paper presents a feedback design technique for energy harvesting applications with single-directional converters. The basic idea is to impose the feedback law

$$i(t) = -Y(t)v(t) \tag{3}$$

where the power-flow directionality constraint requires $Y(t) \geq 0$. Subject to this constraint, $Y(t)$ is modulated as a function of feedback measurements. As such, the technique is fundamentally nonlinear. Comparison of Eqs. (1) and (3) reveals the essential question of the paper—How do we modulate $Y(t)$, subject to the directionality constraint, to enhance power generation beyond that of the best static feedback law?

This problem is very similar to semi-active vibration control problems, in which a damper's viscosity is varied according to a feedback control algorithm in order to suppress vibratory responses more favorably than any constant-damping system. Control algorithms for semi-active vehicle suspensions were first examined by Margolis [16] and Karnopp [17]. Since then, a number of researchers have investigated the advantages of using active and semi-active control strategies for automotive applications [18]. In addition, semi-active control techniques for magnetorheological (MR) dampers, electrorheological (ER) dampers, and other types of controllable dampers have been widely investigated in the literature to mitigate the effects of seismic excitations on multi-story structures [19,20]. The most popular semi-active control synthesis for structural control applications is "clipped-optimal" control, which emulates a fully active LQG control law whenever the desired force is instantaneously dissipative [21]. In a study by Ying et al. [22], the optimal semi-active control law for ER and MR dampers is computed numerically from the stationary solution to the stochastic Bellman equation.

A technique for semi-active feedback control which is guaranteed to outperform constant damping was first proposed for a single-device semi-active system by Tseng and Hedrick [23]. Scruggs et al. in [24] extended those results by developing a stochastic performance-guaranteed theory for systems with an arbitrary number of devices and semi-active or regenerative constraints. That paper illustrated the improvement in performance that can be achieved with a performance-guaranteed controller as compared to the clipped-optimal controllers, as well as compared to linear viscous damping, over a wide range of design objectives. Furthermore, it was also shown in Ref. [24] that the clipped-optimal controller can actually perform worse than the optimal viscous damping when the primary objective is the suppression of accelerations.

The controllers proposed in Refs. [23,24] have the appealing trait that although nonlinear, they are mathematically simple, and could be implemented with analog feedback circuits. This lies in contrast to other options for dealing with constraints in nonlinear optimal control design, such as the use of model predictive control (MPC). As discussed in Ref. [25], even more computationally advanced extensions of the performance-guaranteed controllers proposed here involve simpler control logic than MPC and related techniques. This is especially true due to the fact that MPC algorithms require periodic re-optimization of receding-horizon control trajectories, and these optimizations turn out to be nonconvex for semi-active constraints [26]. Certainly, in the context of a small-scale energy harvester, which almost

certainly requires analog feedback due to restrictions on allowable parasitic dissipation in the control implementation, such computationally intensive techniques are far out of reach.

The techniques proposed in this paper are analogous to those proposed in Refs. [23,24] and discussed above, but the control objective is different. Those studies sought to minimize a positive-definite quadratic performance measure (such as mean-square accelerations or strains), while the present study seeks to maximize average power generation. Furthermore, this study restricts the operating regime of the single-directional power electronic converter to discontinuous conduction in the formulation of the power-flow constraint, resulting in a control problem that is slightly different from semi-active problems. In addition to the synthesis of the performance-guaranteed controller, this paper also presents the energy harvesting equivalent of clipped-optimal semi-active control synthesis. The performances of the controllers are compared for both a single-degree-of-freedom (SDOF) resonant oscillator with electromagnetic coupling, as well as a multi-mode piezoelectric bimorph cantilever beam.

2. The constrained energy harvesting problem

2.1. Harvester and disturbance modeling

Consider the generic conceptual diagram of a single-transducer vibratory energy harvester in Fig. 1. This system consists of a passive electromechanical system with an embedded transducer, which is attached to a power electronic circuit and energy storage. In the more general case, multiple transducers may be considered [13], but here we restrict our attention to single-transducer systems.

We assume that the harvester's electromechanical dynamics can be approximated as linear and finite-dimensional, with state space

$$\dot{\mathbf{x}}_h(t) = \mathbf{A}_h\mathbf{x}_h(t) + \mathbf{B}_h i(t) + \mathbf{G}_h a(t) \tag{4a}$$

$$v(t) = \mathbf{B}_h^T\mathbf{x}_h(t) \tag{4b}$$

where $i(t)$ is the current into the transducer, $a(t)$ is the disturbance acceleration, and $v(t)$ is the voltage at the terminals of the transducer. The power extracted from the harvester by the electronics at time t is $-i(t)v(t)$, where the negative sign is due to the convention that current flowing into the transducer is positive. We assume that the harvester is a passive system, which implies that there always exists a realization such that $\mathbf{B}_h$ has dual participation in both equations above [27]. More specifically, we assume that the driving point impedance of the harvester, as seen from its electrical terminals, is weakly strictly positive real (WSPR). See Ref. [14] for a definition of WSPR, as well as details about its implications for well-posedness of energy harvesting problems.

We assume that the disturbance acceleration $a(t)$ is modeled as white noise that is passed through a finite-dimensional strictly proper, minimum phase filter, i.e.

$$\dot{\mathbf{x}}_a(t) = \mathbf{A}_a\mathbf{x}_a(t) + \mathbf{B}_a w(t) \tag{5a}$$

$$a(t) = \mathbf{C}_a\mathbf{x}_a(t) \tag{5b}$$

where $w(t)$ is white noise with spectral intensity equal to 1. For the purpose of this study, we further assume that disturbance filter is second-order, with the matrices

$$\mathbf{A}_a = \begin{bmatrix} 0 & 1 \\ -\omega_a^2 & -2\zeta_a\omega_a \end{bmatrix}, \quad \mathbf{B}_a = \begin{bmatrix} 0 \\ 2\sigma_a\sqrt{\zeta_a\omega_a} \end{bmatrix}, \quad \mathbf{C}_a = [0 \;\; 1]$$

where ω_a and ζ_a determine the passband of the noise and σ_a is the standard deviation of the disturbance acceleration.

If we combine the harvester and disturbance dynamics such that $\mathbf{x}(t) = [\mathbf{x}_h^T(t) \;\; \mathbf{x}_a^T(t)]^T$, then the augmented system obeys

$$\dot{\mathbf{x}}(t) = \mathbf{A}\mathbf{x}(t) + \mathbf{B}i(t) + \mathbf{G}w(t) \tag{6a}$$

$$v(t) = \mathbf{B}^T\mathbf{x}(t) \tag{6b}$$

with $\mathbf{A}$, $\mathbf{B}$, and $\mathbf{G}$ appropriately defined. We assume that $(\mathbf{A},\mathbf{B}^T)$ is observable and $(\mathbf{A},[\mathbf{B}\;\mathbf{G}])$ is controllable.

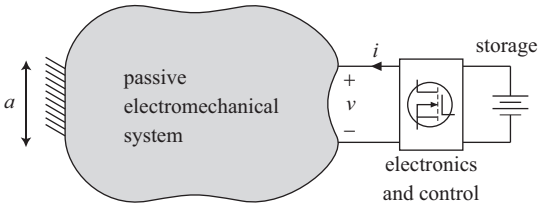

Fig. 1. Generic single-transducer energy harvester.

2.2. Energy harvesting objective

To determine the energy harvesting objective for the system in Eq. (6), we first define the power delivered to storage as the power extracted by the harvester minus the transmission losses in the transducer and power electronic circuitry, i.e.

$$P_S(t) = -i(t)v(t) - P_d(t) \tag{7}$$

where $P_d(t)$ is the transmission dissipation. Typically the expression for $P_d(t)$ is quite complicated, and it depends on the electronic hardware used to realize the controller as well as the manner in which this hardware is operated (e.g., its switching frequency, bus voltage, MOSFET gating voltage, etc.). However, for the purposes of this paper, we will make the simplifying assumption that the power dissipated in the electronics is resistive, i.e., $P_d(t) = Ri^2(t)$. This assumption is made because it yields the most straightforward analysis that still accounts for transmission dissipation in some way. Use of more complicated models for $P_d(t)$ can be viewed as augmenting the theory discussed here.

Given these assumptions, we have that the energy harvesting objective can be defined as the expectation of Eq. (7), i.e.

$$\overline{P}_{\text{gen}} = -\mathcal{E}\left\{ \begin{bmatrix} \mathbf{x} \\ i \end{bmatrix}^T \begin{bmatrix} \mathbf{0} & \frac{1}{2}\mathbf{B} \\ \frac{1}{2}\mathbf{B}^T & R \end{bmatrix} \begin{bmatrix} \mathbf{x} \\ i \end{bmatrix} \right\} \tag{8}$$

Maximization of Eq. (8) is equivalent to a nonstandard LQG optimal control problem where $i(t)$ is treated as the control input. In general, this problem would not be well-posed (i.e., $\overline{P}_{\text{gen}}$ would be unbounded from above). However, it turns out that if the harvester is WSPR, then $\overline{P}_{\text{gen}}$ has a finite maximum over the set of all causal feedback laws [14]. The following theorem introduces the concept of optimal energy harvesting as an LQG control problem.

Theorem 1. *Let the energy harvesting system in Eq. (6) be WSPR. Then for any causal, stabilizing mapping* $\mathbf{x}(t) \mapsto i(t)$

$$\overline{P}_{\text{gen}} = -\mathbf{G}^T\mathbf{Q}\mathbf{G} - R\mathcal{E}\{(\mathbf{F}\mathbf{x} - i)^2\} \tag{9}$$

where $\mathbf{Q} = \mathbf{Q}^T$ *is the solution to the nonstandard Riccati equation*

$$\mathbf{A}^T\mathbf{Q} + \mathbf{Q}\mathbf{A} - \frac{1}{R}\left(\mathbf{Q} + \frac{1}{2}\mathbf{I}\right)\mathbf{B}\mathbf{B}^T\left(\mathbf{Q} + \frac{1}{2}\mathbf{I}\right) = \mathbf{0} \tag{10}$$

and $i(t) = \mathbf{F}\mathbf{x}(t)$ *is the optimal (full-state LQG) feedback control law where*

$$\mathbf{F} = -\frac{1}{R}\mathbf{B}^T\left(\mathbf{Q} + \frac{1}{2}\mathbf{I}\right) \tag{11}$$

If the full state $\mathbf{x}(t)$ *is available for feedback, then the causal limit on power generation is that attained by the above controller, i.e.*

$$\overline{P}_{\text{gen}}^{\text{LQG}} = -\mathbf{G}^T\mathbf{Q}\mathbf{G} \tag{12}$$

Proof. See Ref. [14]. □

2.3. Power-flow constraint

In general, the power electronic hardware necessary to achieve the causal limit $\overline{P}_{\text{gen}} = \overline{P}_{\text{gen}}^{\text{LQG}}$ must be capable of extracting as well as injecting power into the system. Thus, a bi-directional converter such as an H-bridge, which places no restrictions on power directionality, must be used to implement it. When the capabilities of the power electronic converter are restricted, the causal limit is generally unreachable.

As discussed in the introduction, this paper assumes the converter to be single-directional. This implies that the controlled current $i(t)$ must be related to $v(t)$ only through a controllable time-varying admittance $Y(t)$, as in Eq. (3), with restrictions on the range of feasible $Y(t)$ values. More specifically, we investigate the optimal way to implement the relationship in Eq. (3) using the single-directional buck-boost converter in Fig. 2, which is used to regulate $Y(t)$. This type of power electronic converter has been demonstrated for piezoelectric energy harvesting applications in Refs. [10,12].

The buck-boost converter in Fig. 2(a) is controlled via high-frequency pulse-width modulated (PWM) switching of a single MOSFET Q_1. In this paper, we assume that the converter is operated in discontinuous conduction mode (DCM), described as follows. Prior to the leading edge of each switching cycle, inductor L is demagnetized (i.e., its current is zero). Upon the leading edge, Q_1 is gated on, which connects the inductor to the smoothing capacitor C_R, inducing the current in L to rise at a rate $(\mathrm{d}/\mathrm{d}t)i_L(t) \approx V_R/L$. After a fraction D of the total switching period, Q_1 is gated off, causing the inductor current to be routed to the storage bus capacitor C_S and the battery. This causes the inductor current to drop, at a rate $(\mathrm{d}/\mathrm{d}t)i_L(t) \approx -V_S/L$. In DCM, the inductor current drops to zero before the end of the switching cycle, and remains so until Q_1 is gated on again at the leading edge of the next switching cycle. Thus, the inductor current appears as a periodic train of triangular pulses, as is illustrated in Fig. 2(b). During each switching cycle, the total charge transferral is governed by the area underneath the inductor current waveform, which is in turn governed by D.

The advantages of operating a buck-boost converter in DCM are twofold. First, from the point of view of the rectifier voltage V_R, the input impedance of the converter looks resistive at frequencies well below the switching frequency of the converter [28]. Second, the input impedance is approximately decoupled from the behavior of storage voltage V_S. We can

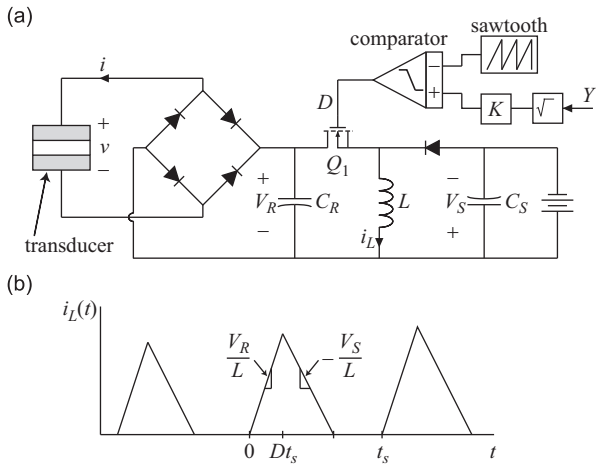

Fig. 2. (a) Energy harvesting transducer interfaced with a full-bridge rectifier and a buck-boost converter. (b) Inductor current $i_L(t)$ with the buck-boost converter operating in DCM.

determine an approximate relationship between the duty cycle and input admittance depending only on inductor L and switching frequency f_{sw}, i.e.

$$D = \sqrt{2YLf_{\mathrm{sw}}} \tag{13}$$

As shown in Fig. 2(a), once a desired admittance Y has been determined, its signal is passed through a square root block and a gain block K to synthesize D. Next, this signal is sent to a comparator along with a sawtooth function, which has a period of $1/f_{\mathrm{sw}}$. The output of the comparator is a voltage signal that is then used to gate Q_1 at the appropriate duty cycle. Refs. [11,12] took similar approaches in which a static admittance was realized by connecting a passive circuit containing two parallel resistors to the non-inverting input of the comparator. With the configurations proposed in those studies, it is shown that the duty cycle of the converter is approximately equal to the ratio of the two resistors. It would be straightforward to augment that circuit such that it would realize the time-varying admittance $Y(t)$.

The single-directionality of the buck-boost converter in Fig. 2(a) restricts the flow of power to extraction, i.e., $i(t)v(t) \le 0$, $\forall t$. Furthermore, an additional constraint must be placed on the circuit such that the operating regime of the buck-boost converter is limited to DCM. Both of these conditions can be enforced by setting $Y(t) \in [0, Y^{\max}]$, where $Y^{\max}$ corresponds to the value of D above which the converter transitions from discontinuous to continuous conduction mode. These two restrictions result in the following power-flow constraint:

$$i(t)v(t) + i^2(t)/Y^{\max} \le 0 \quad \forall t \tag{14}$$

Thus, the constrained energy harvesting problem is to control $Y(t)$ to maximize the energy harvesting performance in Eq. (8) subject to the power-flow constraint in Eq. (14).

2.4. Optimal static admittance

The simplest energy harvesting controller that satisfies the constraint in Eq. (14) is a static admittance (SA), i.e., $Y(t) = Y_c$, $\forall t$, where $Y_c \in [0, Y^{\max}]$. When the electronics are implementing this controller, the current into the transducer is $i(t) = -Y_c v(t)$. Substituting this relationship into Eq. (6) results in the closed-loop dynamics having the form

$$\dot{\mathbf{x}}(t) = [\mathbf{A} - Y_c \mathbf{B}\mathbf{B}^T]\mathbf{x}(t) + \mathbf{G}w(t) \tag{15}$$

For this linear, time-invariant system, finding the optimal Y_c which maximizes the energy harvesting performance in Eq. (8) is summarized by the following theorem.

Theorem 2. *For the system described by Eq. (15), the energy harvesting performance is*

$$\overline{P}_{\mathrm{gen}}^{\mathrm{SA}} = -\mathbf{G}^T\mathbf{P}\mathbf{G} \tag{16}$$

where $\mathbf{P} = \mathbf{P}^T$ *is the unique solution to the Lyapunov equation*

$$[\mathbf{A} - Y_c\mathbf{B}\mathbf{B}^T]^T\mathbf{P} + \mathbf{P}[\mathbf{A} - Y_c\mathbf{B}\mathbf{B}^T] + \mathbf{B}(-Y_c + Y_c^2 R)\mathbf{B}^T = \mathbf{0} \tag{17}$$

Furthermore

$$\frac{\partial \overline{P}_{\mathrm{gen}}^{\mathrm{SA}}}{\partial Y_c} = -2\mathbf{B}^T\left(\mathbf{P} + \left[\frac{1}{2} - RY_c\right]\mathbf{I}\right)\mathbf{\Sigma}\mathbf{B} \tag{18}$$

where the stationary covariance matrix $\boldsymbol{\Sigma} = \mathcal{E}\{\mathbf{x}\mathbf{x}^T\}$ *is found by solving the Lyapunov equation*

$$[\mathbf{A} - Y_c\mathbf{B}\mathbf{B}^T]\boldsymbol{\Sigma} + \boldsymbol{\Sigma}[\mathbf{A} - Y_c\mathbf{B}\mathbf{B}^T]^T + \mathbf{G}\mathbf{G}^T = \mathbf{0} \tag{19}$$

Proof. This is a standard result from linear-quadratic control theory and its proof can be found in Ref. [29]. □

Because the system only has one design parameter (i.e., Y_c) in this case, the most straightforward way to optimize $\overline{P}_{\text{gen}}$ is via a one-dimensional line search. For example, the bisection algorithm will converge rapidly to the optimal Y_c, given **A**, **B**, **G**, and R. However, for more complicated systems involving multiple transducers, the optimal SA can be found through a first-order gradient descent algorithm [30].

3. Nonlinear power-flow-constrained control

This section extends the results presented for the SA controller, in which $Y(t)$ is adjusted in response to feedback measurements of the full system state, to further increase $\overline{P}_{\text{gen}}$. Because it is more difficult to find analytical expressions for $\overline{P}_{\text{gen}}$ (such as in Eq. (16)) for time-varying $Y(t)$, we relax the control design objective to the design of controllers for which sufficient conditions exist to guarantee that $\overline{P}_{\text{gen}} \geq \overline{P}^{\text{SA}}_{\text{gen}}$. In other words, the feedback controller is guaranteed to generate at least as much power as the optimal SA controller.

3.1. Performance-guaranteed control

Theorem 3. *For the linear system in Eq. (6), let* Y_c *be a feasible SA controller. Let* $\mathbf{x}(t) \mapsto i(t)$ *be any causal mapping, such that the closed-loop system is globally bounded-input bounded-state stable. Then, in stationary response, the energy harvesting performance is*

$$\overline{P}_{\text{gen}} = -\mathbf{G}^T\mathbf{P}\mathbf{G} + R\mathcal{E}\{(\mathbf{K}\mathbf{x} + Y_c v)^2 - (\mathbf{K}\mathbf{x} - i)^2\} \tag{20}$$

where $\mathbf{P} = \mathbf{P}^T$ *is the unique stabilizing solution to Eq. (17) and*

$$\mathbf{K} = -\frac{1}{R}\mathbf{B}^T\left(\mathbf{P} + \frac{1}{2}\mathbf{I}\right) \tag{21}$$

Proof. We begin by multiplying Eq. (17) by $\mathbf{x}^T(t)$ on the left and $\mathbf{x}(t)$ on the right, taking the expectation, and subtracting from Eq. (8), which gives

$$\overline{P}_{\text{gen}} = -\mathcal{E}\{\mathbf{x}^T[\mathbf{A} - Y_c\mathbf{B}\mathbf{B}^T]^T\mathbf{P}\mathbf{x} + \mathbf{x}^T\mathbf{P}[\mathbf{A} - Y_c\mathbf{B}\mathbf{B}^T]\mathbf{x}\} - \mathcal{E}\{\mathbf{x}^T\mathbf{B}(-Y_c + Y_c^2R)\mathbf{B}^T\mathbf{x}\} - \mathcal{E}\{\tfrac{1}{2}\mathbf{B}^T\mathbf{x}i\} - \mathcal{E}\{\tfrac{1}{2}\mathbf{x}^T\mathbf{B}i\} - \mathcal{E}\{Ri^2\} \tag{22}$$

Some rearranging and use of Eq. (21) results in

$$\overline{P}_{\text{gen}} = -\mathcal{E}\{[\mathbf{A}\mathbf{x} + \mathbf{B}i]^T\mathbf{P}\mathbf{x} + \mathbf{x}^T\mathbf{P}[\mathbf{A}\mathbf{x} + \mathbf{B}i]\} + R\mathcal{E}\{(\mathbf{K}\mathbf{x} + Y_c v)^2 - (\mathbf{K}\mathbf{x} - i)^2\} \tag{23}$$

To show that the first term on the right-hand side of Eq. (23) is equal to $-\mathbf{G}^T\mathbf{P}\mathbf{G}$, we first define $\psi = \mathbf{x}^T(t)\mathbf{P}\mathbf{x}(t)$. Then, adopting the Itô convention of stochastic calculus [31], we have that

$$\frac{\mathrm{d}\psi}{\mathrm{d}t} = \frac{\partial\psi}{\partial t} + (\nabla_{\mathbf{x}}\psi)(\mathbf{A}\mathbf{x}(t) + \mathbf{B}i(t)) + (\nabla_{\mathbf{x}}\psi)\mathbf{G}w(t) + \frac{1}{2}\mathbf{G}^T(\nabla_{\mathbf{x}} \otimes \nabla_{\mathbf{x}}\psi)\mathbf{G} \tag{24}$$

where $\nabla_{\mathbf{x}}$ is the gradient with respect to the variable $\mathbf{x}$, and $\nabla_{\mathbf{x}} \otimes \nabla_{\mathbf{x}}$ is the Hessian. Evaluating these for our definition of ψ, and taking expectations of both sides, gives

$$\mathcal{E}\left\{\frac{\mathrm{d}}{\mathrm{d}t}\mathbf{x}^T\mathbf{P}\mathbf{x}\right\} = \mathcal{E}\{[\mathbf{A}\mathbf{x} + \mathbf{B}i]^T\mathbf{P}\mathbf{x} + \mathbf{x}^T\mathbf{P}[\mathbf{A}\mathbf{x} + \mathbf{B}i]\} + \mathcal{E}\{\mathbf{x}^T\mathbf{P}\mathbf{G}w + \mathbf{G}^T\mathbf{P}\mathbf{x}w\} + \mathbf{G}^T\mathbf{P}\mathbf{G} \tag{25}$$

In stationarity the left-hand side of Eq. (25) is 0. Furthermore, by the Itô convention, the second-to-last term on the right-hand side of Eq. (25) is also 0 because the mapping $\mathbf{x}(t) \mapsto i(t)$ is causal. This completes the proof. □

In the above theorem, we see that the expression for $\overline{P}_{\text{gen}}$ is a summation of two terms. The first of these is actually the value of $\overline{P}_{\text{gen}}$ when $Y(t) = Y_c$. The second term in Eq. (20) (i.e., the expectation) does not in general have a closed form. In the formulation of the PG feedback controller, $Y(t)$ is chosen such that the term in the expectation is positive at every time, thus ensuring a positive expectation and enhanced power generation.

Theorem 4. *For the system in Eq. (15), let* $Y_c^\star$ *be the optimal SA, and let* $\overline{P}^{\text{SA}^\star}_{\text{gen}}$ *be its performance. Also, let* **P** *and* **K** *be determined by Eqs. (17) and (21) with* $Y_c = Y_c^\star$*. Then the following control law*

$$Y(t) = \underset{\tilde{Y} \in [0, Y^{\max}]}{\arg\min}\{R(\mathbf{K}\mathbf{x}(t) + \tilde{Y}v(t))^2\} \tag{26}$$

adheres to the performance-guaranteed (PG) power generation inequality

$$\overline{P}_{\text{gen}}^{\text{PG}} \geq \overline{P}_{\text{gen}}^{\text{SA}\star} \tag{27}$$

Proof. Substitution of Eq. (3) into Eq. (20) gives

$$\overline{P}_{\text{gen}}^{\text{PG}} = \overline{P}_{\text{gen}}^{\text{SA}\star} + R\mathcal{E}\{(\mathbf{K}\mathbf{x}+Y_c^{\star}v)^2-(\mathbf{K}\mathbf{x}+Yv)^2\} \tag{28}$$

Thus, the control law in Eq. (26) gives performance

$$\overline{P}_{\text{gen}}^{\text{PG}} = \overline{P}_{\text{gen}}^{\text{SA}\star} + R\mathcal{E}\left\{(\mathbf{K}\mathbf{x}+Y_c^{\star}v)^2-\min_{\tilde{Y}\in[0,Y^{\max}]}(\mathbf{K}\mathbf{x}+\tilde{Y}v)^2\right\} \tag{29}$$

The term in the brackets is nonnegative at every time, because $Y_c^{\star} \in [0,Y^{\max}]$. Thus, its expectation is nonnegative, completing the proof. □

The control law in Eq. (26) may also be expressed directly in terms $i(t)$. We begin by defining the unconstrained feedback signal $i_u(t)$ as

$$i_u(t) = \mathbf{K}\mathbf{x}(t) \tag{30}$$

Then the time-varying admittance imposes a corresponding feedback relationship for $i(t)$ as

$$i(t) = \underset{\tilde{i}v+\tilde{i}^2/Y^{\max}\leq 0}{\arg\min}\ \{R(\tilde{i}(t)-i_u(t))^2\} \tag{31}$$

where the feasibility of the $\tilde{i}(t)$ is determined by the power-flow constraint in Eq. (14). Thus, $i(t)$ tracks the unconstrained feedback signal $i_u(t)$ if it is feasible, and if not $i_u(t)$ is clipped to the feasible region. The clipping action is evaluated as a saturation function of $i_u(t)$, i.e.

$$i(t) = \underset{i_uv+i_u^2/Y^{\max}\leq 0}{\text{sat}}\{i_u(t)\} = \begin{cases} i_u(t) & : i_u(t)v(t)+i_u^2(t)/Y^{\max}\leq 0 \\ 0 & : i_u(t)v(t)+i_u^2(t)/Y^{\max}>0 \quad \text{and} \quad i_u(t)v(t)>0 \\ -Y^{\max}v(t) & : \text{otherwise} \end{cases} \tag{32}$$

For more complicated problems involving multiple transducers, the clipping action that instantaneously minimizes the tracking error in Eq. (31) may not be a saturation function. Interested readers should see Ref. [24], which presents a more detailed clipping procedure for a system with an arbitrary number of transducers and semi-active or regenerative constraints.

3.2. Clipped-optimal control

It turns out that the control formulation in Eq. (32) is identical in form to that of clipped-optimal (CO) control. Replacing the PG gain matrix $\mathbf{K}$ with the LQG gain matrix $\mathbf{F}$ in Eq. (30) and updating $i_u(t)$ in Eq. (32) results in the CO controller. The performance of an energy harvester implementing the CO controller can be expressed as

$$\overline{P}_{\text{gen}}^{\text{CO}} = -\mathbf{G}^T\mathbf{Q}\mathbf{G}-R\mathcal{E}\{(i-i_u)^2\} \tag{33}$$

where $i_u(t) = \mathbf{F}\mathbf{x}(t)$. The first term in the summation above is equal to the performance of the optimal LQG controller, while the second term is the depreciation in performance due to the fact that $i(t)$ is constrained to a feasible region. The CO controller attempts to minimize the expectation in the second term at every time instant, resulting in the same controller as Eq. (32) but with $i_u(t)$ formulated as above, as based on the LQG gain matrix.

In other words, the CO controller attempts to get as close as possible to realizing the fully active, unconstrained optimal feedback law from Theorem 1. However, there is in general no guarantee for how close it actually gets to doing this, i.e., there is no analytical bound on the second term in Eq. (33).

4. Examples

4.1. Electromagnetic energy harvester

Consider the energy harvesting system in Fig. 3(a), consisting of the electromagnetic transducer embedded within a single-degree-of-freedom (SDOF) resonant oscillator. The SDOF oscillator has a mass m_s, damping c_s, and stiffness k_s. The electromagnetic transducer consists of a ballscrew coupled to a permanent magnet synchronous machine and has equivalent mass m_d, damping c_d, stiffness k_d, and electromechanical coupling c_e. The harvester state vector can be partitioned as

$$\mathbf{x}_h(t) = [\sqrt{k}r(t)\ \ \sqrt{m}\dot{r}(t)]^T \tag{34}$$

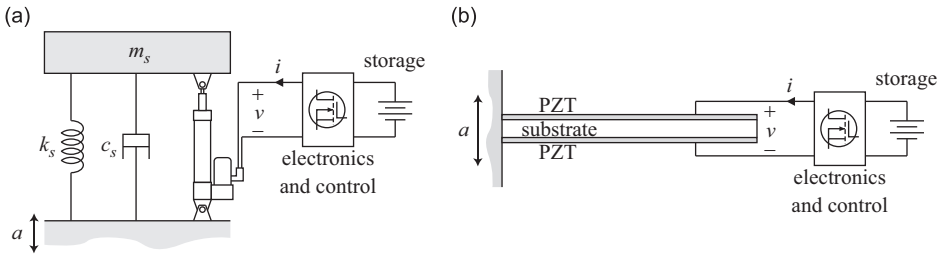

Fig. 3. Passive energy harvesting systems: (a) SDOF oscillator with an electromagnetic transducer and (b) piezoelectric bimorph cantilever beam.

Table 1
Parameter values for the electromagnetic energy harvester.

Parameter	Value	Parameter	Value
m_s	3000 kg	k_d	630 N/m
c_s	395 N s/m	c_e	453 N/A
k_s	3×10^4 N/s	ω_a	3.14 rad/s
m_d	20 kg	σ_a	0.18 m/s^2
c_d	575 N s/m	$Y^{\max}$	0.05 Ω^{-1}

where $r(t)$ is the relative displacement of the moving mass. For this realization, the coefficient matrices for the system are

$$\mathbf{A}_h=\begin{bmatrix}0 & \sqrt{k/m}\\ -\sqrt{k/m} & -c/m\end{bmatrix},\quad \mathbf{B}_h=\begin{bmatrix}0\\ c_e/\sqrt{m}\end{bmatrix},\quad \mathbf{G}_h=\begin{bmatrix}0\\ m_s/\sqrt{m}\end{bmatrix}$$

where $m=m_s+m_d$, $c=c_s+c_d$, and $k=k_s+k_d$.

For the example considered in this paper, the parameters for the SDOF oscillator and electromagnetic transducer are given in Table 1. These values correspond to the experimental system that was investigated in Ref. [32]. For simplicity, we neglect the Coulomb friction force and other nonlinear dissipative forces that are present in the actual device. The disturbance parameter ζ_a and the transmission dissipation R will be treated as adjustable parameters. In addition, we set the maximum admittance that can be imposed by the electronics (i.e., $Y^{\max}$) at 0.05 Ω^{-1}. For an ideal system $Y^{\max}$ must be less than or equal to $1/R$. Therefore, setting $Y^{\max}=0.05\ \Omega^{-1}$ is a conservative approximation of $Y^{\max}$ for the values of R investigated in this example (except for the limiting case in which $R=20\ \Omega$). In a physical system, $Y^{\max}$ can easily be calculated using the known values of the power electronic converter (i.e., inductance, switching frequency, etc.). However, designing an actual buck-boost converter in order to calculate $Y^{\max}$ is beyond the scope of this paper.

We begin by determining an expression for the PG feedback controller. It turns out that the solution to the Lyapunov equation in Eq. (17) has a special form for this example, i.e.

$$\mathbf{P}=\begin{bmatrix}P_{22} & 0 & P_{13} & 0\\ 0 & P_{22} & 0 & P_{24}\\ P_{13} & 0 & P_{33} & 0\\ 0 & P_{24} & 0 & P_{44}\end{bmatrix} \tag{35}$$

We can explicitly solve for $\{P_{22},P_{33},P_{44},P_{13},P_{24}\}$ analytically in terms of the harvester and disturbance parameters. The corresponding PG gain matrix is

$$\mathbf{K}=\left[0\ \ -\frac{c_e}{\sqrt{m}R}\left(P_{22}+\frac{1}{2}\right)\ \ 0\ \ -\frac{c_e}{\sqrt{m}R}P_{24}\right] \tag{36}$$

where

$$P_{22}=\frac{c_e^2(-Y_c^\star+Y_c^\star 2R)}{2(c+c_e^2Y_c^\star)} \tag{37a}$$

$$P_{24}=\frac{c_e^2m_s\sqrt{m}(-Y_c^\star+Y_c^\star 2R)}{2(c+c_e^2Y_c^\star)(c+c_e^2Y_c^\star+2m\zeta_a\omega_a)} \tag{37b}$$

Given the expression for $\mathbf{K}$ in Eq. (36) and the fact that $v(t)=c_e\dot{x}(t)$, we can express the PG control law as

$$i(t)=\underset{iv+i^2/Y^{\max}\le 0}{\text{sat}}\{K_v v(t)+K_a a(t)\} \tag{38}$$

where K_v and K_a are the nonzero components of the PG gain matrix $\mathbf{K}$. Recognizing that $i(t) = -Y(t)v(t)$, this implies that the equation to determine the time-varying admittance for this controller directly is

$$Y(t) = \underset{[0,Y^{\max}]}{\text{sat}}\left\{-K_v - K_a \frac{a(t)}{v(t)}\right\} \tag{39}$$

The argument in the brackets consists of a constant term, plus a term that varies with the ratio $a(t)/v(t)$. It is this variable term that is responsible for the improvement in performance over the optimal SA controller. Furthermore, we note that an experimental implementation of this controller only requires feedback measurements of the transducer voltage and disturbance acceleration. A simulation example of the PG controller is provided over a time span of 60 seconds in Fig. 4. For this example, we illustrate the equivalent time-varying admittance resulting from this controller in Fig. 4(a) and the power delivered to storage in Fig. 4(b). The power-flow constraint in Eq. (14) is successfully enforced for this example, as shown in Fig. 4(c).

Next, we determine an expression for the CO controller. It turns out that the solution $\mathbf{Q}$ to the Riccati equation in Eq. (10) also has a special form for the augmented state space defined in this example. Thus, we can utilize the decoupling properties of the Riccati equation for energy harvesters adhering to Eq. (6), which is presented in more detail in Ref. [15], to determine the CO controller. The admittance resulting from the CO control law can be written as

$$Y(t) = \underset{[0,Y^{\max}]}{\text{sat}}\left\{-F_v - F_a \frac{a(t)}{v(t)}\right\} \tag{40}$$

where F_v and F_a are the nonzero components of the LQG gain matrix $\mathbf{F}$.

To compare the performances of the PG controller to the CO controller, we plot the ratios of their performances divided by the performance of the SA case. This ratio represents the marginal improvement afforded by the control system over the optimal SA. For reference, we also include the ratio of the performance of the unconstrained LQG controller divided by the performance of the SA controller. These ratios are plotted over a range of disturbance bandwidths (i.e., $\zeta_a \in [0,1]$) and for several transmission dissipation values. Because the performances of the PG and CO controllers do not have closed-form solutions, we simulate the SDOF system for 3000 seconds at a sample of rate of 100 Hz in order to calculate an approximate stationary solution for $\overline{P}_{\text{gen}}$.

In Fig. 5, we see that the CO controller performs slightly better than the PG controller for all values of R. From this result, it can be concluded that CO controllers perform well in terms of the energy harvesting performance measure for single-mode systems. For larger values of R, we notice that the PG and CO controllers converge to the same performance, which can be clearly seen in Fig. 5(d). In the narrowband limit (i.e., as $\zeta_a \to 0$), the performance ratios of all of the controllers approach unity. As pointed out in Ref. [15], this is due to the fact that for the system under consideration, the velocity and disturbance acceleration gains are the only gains required for the feedback control laws. As such, $v(t)$ and $a(t)$ become purely sinusoidal and exactly in phase in the narrowband limit, which means that knowledge of both is redundant. This result therefore verifies that in the narrowband limit, the optimal causal $\overline{P}_{\text{gen}}$ is actually attained by the optimal static admittance.

Finally, we plot the performance of the various controllers for varying the $Y^{\max}$ values in Fig. 6. In this plot, we set $\zeta_a = 0.2$ and $R = 5\ \Omega$ and compare the average power generated by the LQG, SA, CO, and PG controllers. As $Y^{\max} \to 0$, we see that the performance of the SA, PG, and CO controllers approach zero. This limit corresponds to the case where the electronics can only impose an open circuit condition on the transducer, which results in no average power generated by the system. For increasing values of $Y^{\max}$, the CO controller performs slightly better than the PG controller and both the

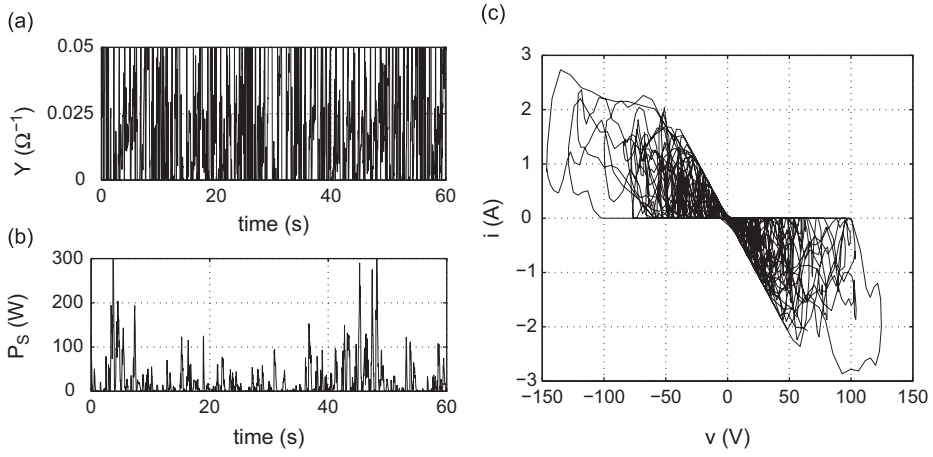

Fig. 4. Example simulation using the PG controller for $R = 5\ \Omega$ and $\zeta_a = 0.5$: (a) $Y(t)$ vs. time, (b) $P_S(t)$ vs. time, and (c) $i(t)$ vs. $v(t)$.

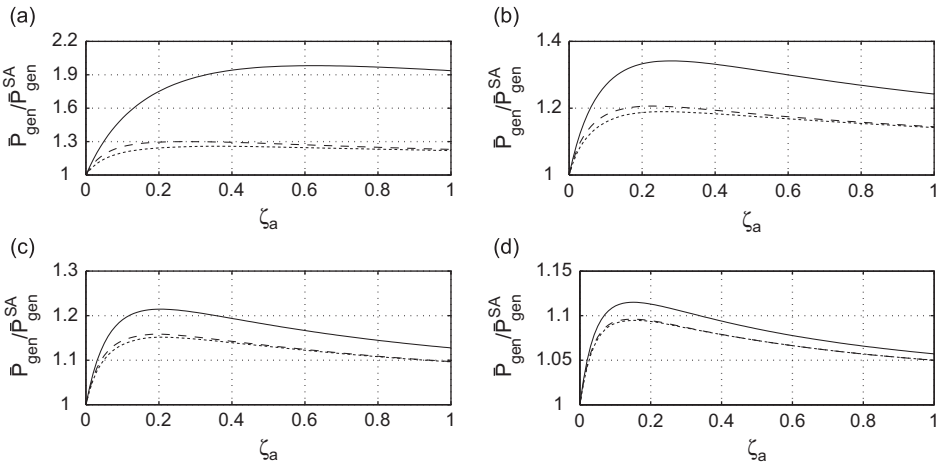

Fig. 5. Ratio of $\overline{P}_{\text{gen}}/\overline{P}^{\text{SA}}_{\text{gen}}$ vs. ζ_a for $\overline{P}_{\text{gen}}=\overline{P}^{\text{LQG}}_{\text{gen}}$ (solid), $\overline{P}_{\text{gen}}=\overline{P}^{\text{CO}}_{\text{gen}}$ (dashed), and $\overline{P}_{\text{gen}}=\overline{P}^{\text{PG}}_{\text{gen}}$ (dotted): (a) $R=1\ \Omega$, (b) $R=5\ \Omega$, (c) $R=10\ \Omega$, and (d) $R=20\ \Omega$.

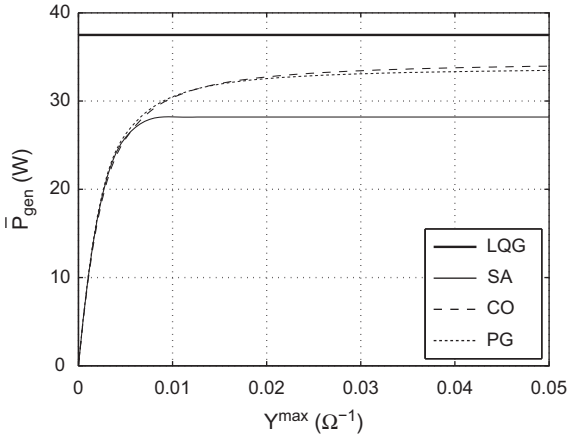

Fig. 6. Comparison of $\overline{P}_{\text{gen}}$ vs. $Y^{\max}$ for $\zeta_a=0.2$ and $R=5\ \Omega$.

CO and PG controllers perform better than the SA controller. The most important result of this analysis is that the performances of the SA, CO, and PG controllers approach constant values as $Y^{\max}$ increases. This implies that there is a critical value of $Y^{\max}$ that must be achieved by the electronics in order to fully realize the potential performance offered by these control laws.

4.2. Piezoelectric energy harvester

Next, consider the bimorph piezoelectric cantilever beam in Fig. 3(b). We assume that the piezoelectric patches are made of lead zirconate titanate (PZT), which are bonded to a flexible substrate. Using standard Rayleigh–Ritz techniques to arrive at a finite-dimensional beam model, and imposing classical mechanical damping, the harvester state vector can be partitioned as

$$\mathbf{x}_h(t)=[q_1(t)\ \ \dot{q}_1(t)\ \ \cdots\ \ q_N(t)\ \ \dot{q}_N(t)\ \ p(t)]^T \tag{41}$$

where $\{q_k(t),\dot{q}_k(t)\}$ are generalized mechanical position and velocity coordinates of vibratory mode k, and $p(t)$ is normalized piezoelectric voltage. Given these coordinates, a realization exists for which

$$\mathbf{A}_h=\begin{bmatrix}\boldsymbol{\Omega} & \boldsymbol{\Theta}\\ -\boldsymbol{\Theta}^T & -1/\tau\end{bmatrix},\quad \mathbf{B}_h=\begin{bmatrix}\mathbf{0}\\ \beta\end{bmatrix},\quad \mathbf{G}_h=\begin{bmatrix}\mathbf{N}\\ 0\end{bmatrix}$$

and where the further partitionings are made in modal form, i.e.

$$\mathbf{\Omega} = \underset{k=1\ldots N}{\text{diag}}\left\{\begin{bmatrix} 0 & \omega_k \\ -\omega_k & -2\zeta_k\omega_k \end{bmatrix}\right\}, \quad \mathbf{\Theta} = \underset{k=1\ldots N}{\text{col}}\left\{\begin{bmatrix} 0 \\ \theta_k \end{bmatrix}\right\}, \quad \mathbf{N} = \underset{k=1\ldots N}{\text{col}}\left\{\begin{bmatrix} 0 \\ \eta_k \end{bmatrix}\right\}$$

For the example considered in this paper, the parameters for the piezoelectric bimorph cantilever beam are given in Table 2. These correspond to the transducer studied in Ref. [33] with the exception of τ, which was assumed infinite in that study and is given a finite value here to reflect finite dielectric leakage of the piezoelectric transducer.

We assume that the disturbance state space matrices $\mathbf{A}_a$, $\mathbf{B}_a$, and $\mathbf{C}_a$ are the same as the previous example with σ_a listed in Table 2. In addition, the parameters ζ_a, ω_a, and R are treated as adjustable variables. We set $Y^{\max} = 0.01\ \Omega^{-1}$, which corresponds to the inverse of the maximum R value investigated in this example. Unlike the previous example, the augmented state space for this example results in LQG, CO, and PG control laws that do not decouple and the entire augmented state vector $\mathbf{x}(t)$ is required for feedback. The feedback gain matrices $\mathbf{K}$ and $\mathbf{F}$ must be computed numerically and do not have any entries that are identically zero.

For this example, we begin by plotting the ratio of the performance achieved by the LQG, CO, and PG controllers divided by the performance of the SA controller. Since the performances of the PG and CO controllers do not have closed-form solutions, we simulate the piezoelectric system for 40 seconds at a sample of rate of 10 kHz in order to calculate an approximate stationary solution for $\overline{P}_{\text{gen}}$. The plots in Fig. 7 illustrate these ratios over a range of disturbance bandwidths for $\omega_a = \omega_1$ (i.e., the passband of the disturbance filter is centered at the first natural frequency of the beam). From these plots we see that the PG controller outperforms the CO controller for all values of R. Furthermore, in the narrowband limit as $\zeta_a \to 0$ we see that the ratios are not equal to unity because for a narrowband disturbance, $\overline{P}_{\text{gen}}$ is maximized by a passive linear admittance consisting of a resistor and a reactive component (i.e., an inductor). In other words, the optimal controller at the narrowband limit is no longer just a static admittance.

Next, we plot the same performance ratios for the case where the passband of the disturbance filter is centered at the second natural frequency of the beam, i.e., $\omega_a = \omega_2$. A plot of the performance ratios for this case with increasing values of R can be seen in Fig. 8. Again, we notice that the PG controller outperforms the CO controller for all values of R and that the ratios are not equal to unity in the narrowband limit. We can conclude that efficient harvesting energy from systems excited at higher modes requires some type of feedback control.

Table 2
Parameter values for the piezoelectric energy harvester.

Parameter	Value	Parameter	Value
ω_1	241 rad/s	θ_3	$375\ \text{s}^{-1}$
ω_2	1510 rad/s	η_1	$-0.0820\ \sqrt{\text{kg}}$
ω_3	4220 rad/s	η_2	$-0.0454\ \sqrt{\text{kg}}$
ζ_1	0.010	η_3	$-0.0267\ \sqrt{\text{kg}}$
ζ_2	0.0435	τ	2 s
ζ_3	0.121	β	$1770\ \sqrt{\Omega/\text{s}}$
θ_1	$65.8\ \text{s}^{-1}$	σ_a	9.81 m/s
θ_2	$-228\ \text{s}^{-1}$	$Y^{\max}$	$0.01\ \Omega^{-1}$

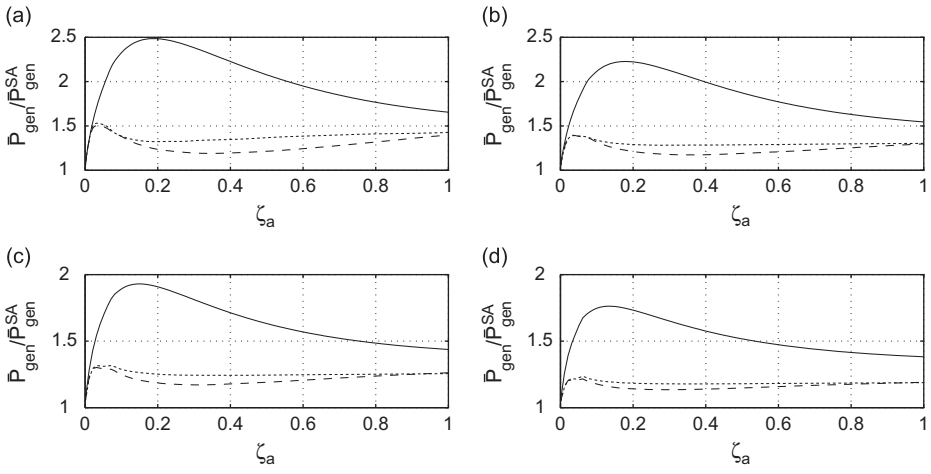

Fig. 7. Ratio of $\overline{P}_{\text{gen}}/\overline{P}^{\text{SA}}_{\text{gen}}$ vs. ζ_a for $\overline{P}_{\text{gen}} = \overline{P}^{\text{LQG}}_{\text{gen}}$ (solid), $\overline{P}_{\text{gen}} = \overline{P}^{\text{CO}}_{\text{gen}}$ (dashed), and $\overline{P}_{\text{gen}} = \overline{P}^{\text{PG}}_{\text{gen}}$ (dotted), and setting $\omega_a = \omega_1$: (a) $R = 5\ \Omega$, (b) $R = 10\ \Omega$, (c) $R = 50\ \Omega$, and (d) $R = 100\ \Omega$.

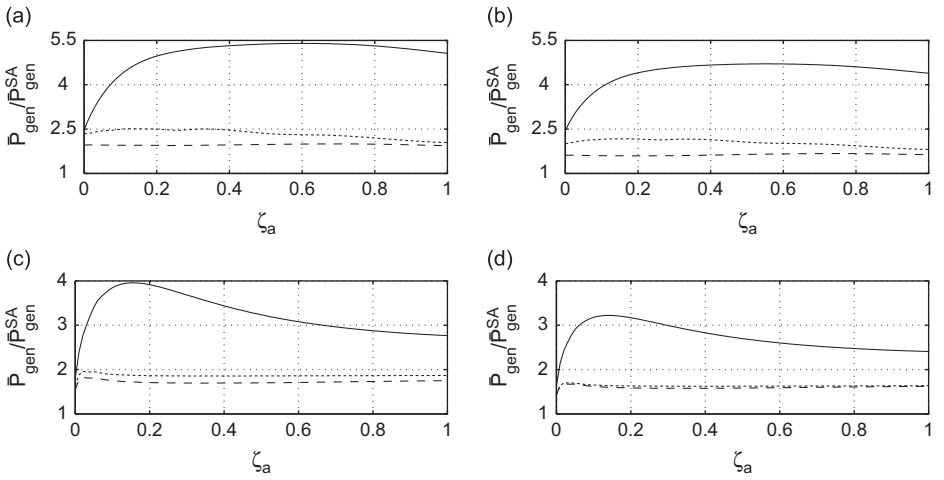

Fig. 8. Ratio of $\overline{P}_{gen}/\overline{P}^{SA}_{gen}$ vs. ζ_a for $\overline{P}_{gen}=\overline{P}^{LQG}_{gen}$ (solid), $\overline{P}_{gen}=\overline{P}^{CO}_{gen}$ (dashed), and $\overline{P}_{gen}=\overline{P}^{PG}_{gen}$ (dotted), and setting $\omega_a=\omega_2$: (a) $R=5\,\Omega$, (b) $R=10\,\Omega$, (c) $R=50\,\Omega$, and (d) $R=100\,\Omega$.

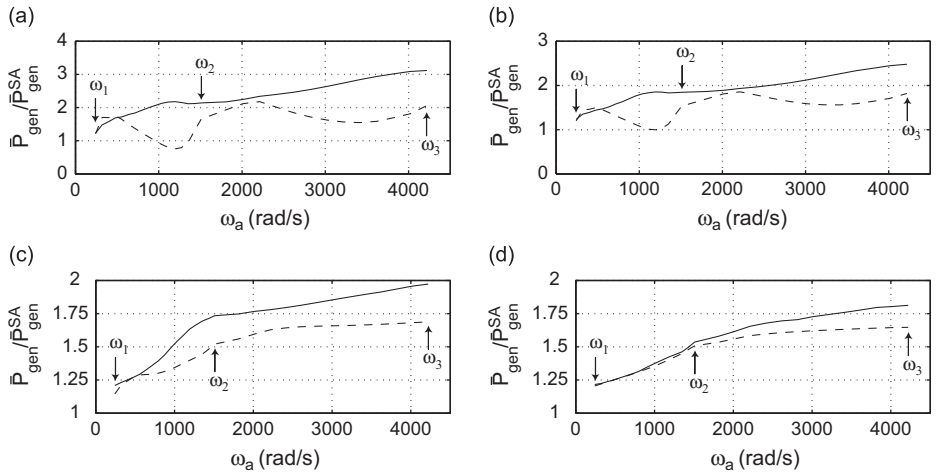

Fig. 9. Ratio of $\overline{P}_{gen}/\overline{P}^{SA}_{gen}$ vs. ω_a for $\overline{P}_{gen}=\overline{P}^{CO}_{gen}$ (dashed) and $\overline{P}_{gen}=\overline{P}^{PG}_{gen}$ (solid), and setting $R=10\,\Omega$: (a) $\zeta_a=0.05$, (b) $\zeta_a=0.1$, (c) $\zeta_a=0.5$, and (d) $\zeta_a=1$.

In order to further compare the CO and PG controllers, the plot in Fig. 9 illustrates the performance ratios over a range of disturbance passband values, i.e., $\omega_a\in[\omega_1,\omega_3]$. For these plots, we fix $R=10\,\Omega$ and compare the performance ratios for ζ_a values of 0.05, 0.1, 0.5, and 1. It is important to point out in Fig. 9(a) that there is a range of ω_a values which result in $\overline{P}^{CO}_{gen}/\overline{P}^{SA}_{gen}<1$. In this range, the CO controller actually performs worse than the optimal SA controller. Furthermore, we see that the performance of the PG controller is much better than the performance of the CO controller in range $\omega_a\in[\omega_2,\omega_3]$, for all values of ζ_a. We can therefore conclude that the PG controller is able to harvest more energy from multi-mode systems, especially when the passband of the disturbance is centered at frequencies greater than the first natural frequency of the system.

Finally, we plot the performance of the various controllers for varying Y^{max} values in Fig. 10. In this plot, we set $\zeta_a=0.2$ and $R=5\,\Omega$ and compare the average power generated by the LQG, SA, CO, and PG controllers. The plot in Fig. 10(a) is for $\omega_a=\omega_1$ while the plot in Fig. 10(b) is for $\omega_a=\omega_2$. As $Y^{max}\to 0$, we see that the performance of the SA, PG, and CO controllers approach zero for both plots. However, unlike the previous example, we see that the PG controller performs slightly better than the CO controller for increasing values of Y^{max}. Again, we see that the performance of the SA, CO, and PG controllers approach constant values as Y^{max} increases.

5. Conclusions and discussion

In the application of power-flow-constrained feedback control laws to maximize power generation, the increased complexity of such technology must be justified by some assurance that they can outperform simpler techniques. Toward

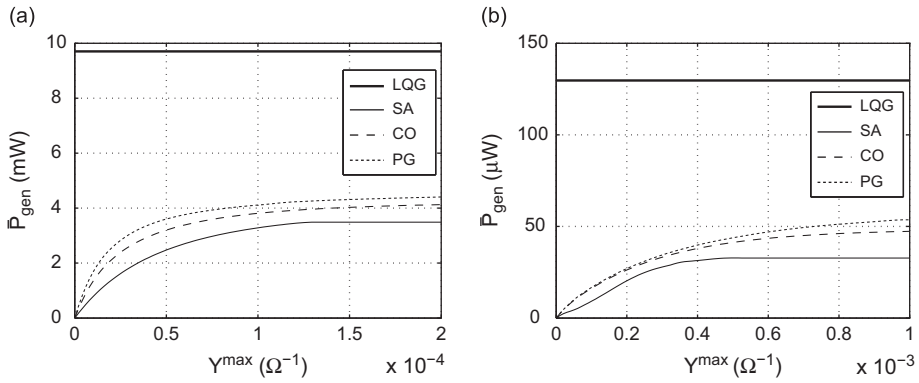

Fig. 10. Comparison of $\overline{P}_{\text{gen}}$ vs. $Y^{\max}$ for $\zeta_a = 0.2$ and $R = 5\,\Omega$: (a) $\omega_a = \omega_1$ and (b) $\omega_a = \omega_2$.

this end, this study has presented a PG control design technique which results in consistent performance trends under the power generation performance measure. The main result of this analysis is that PG controllers can be designed to outperform the optimal performance achievable by the SA controller. However, there is in general no analytical expression for the margin of improvement. By comparison, CO controllers do not possess theoretical bounds on the performance and, in some cases, perform worse than the optimal SA controller.

The controllers presented in this study were simulated for both an electromagnetic energy harvester as well as a piezoelectric energy harvester. For the electromagnetic example, the CO controller can harvest slightly more average power than the PG controller. We can conclude that for single-mode systems, using a CO controller is advantageous in terms of the energy harvesting performance. However, this result contrasts with the piezoelectric example, which consists of a cantilever beam with three distinct modes. For multi-modal energy harvesting systems, PG controllers are much more effective at generating power than CO controllers, especially for scenarios in which the disturbance passband is centered at frequencies greater than the first natural frequency of the harvester. Finally, this study showed that the performances of the SA, CO, and PG controllers approach constant values as the upper bound on the maximum feasible admittance of the electronics increases. This result is important because of its implications for the design of power electronic converters capable of implementing a given feedback law.

We close this paper by mentioning a few long-standing open issues pertaining to PG and CO controllers, which have persisted in the literature on semi-active damping control, and which are equally relevant to energy harvesting problems. First, we note that all the theory discussed in this paper is in the context of state feedback, which is generally impractical. We have shown that in a number of basic examples, the harvester can be tuned such that only easy-to-sense states (i.e.,voltage and acceleration) have nonzero feedback gains, and this implies that knowledge of only these states is required to implement the optimal control law. Nonetheless, even in this case an observer-based controller may still be a preferable approach for estimating some of these states. In the literature on semi-active control, there have indeed been a few investigations on extension of this theory to accommodate an observer [34,35]. In particular, Ref. [35] derives analogous PG controllers for semi-active output-feedback systems, but these control designs are computationally demanding, and require that $Y(t)$ be chosen at each time to explicitly balance the tasks of observation and response suppression. At present, there is no known separation principle for PG controllers (or CO controllers, for that matter).

Second, we note that in this paper, we have deferred questions as to the robustness of PG (as well as CO) controllers for future work. It seems only one statement can be made with certainty: For harvesters adhering to the WSPR modeling assumptions made here, PG and CO controllers are unconditionally robust to instability, because they do not permit power to flow to the harvester. Indeed, this stability robustness trait is one of the appeals of semi-active vibration control systems. However, there is not at present a clear understanding of the degree to which parameter uncertainty (both in the disturbance and harvester models) degrades power generation performance. Also, it is unclear whether the special structure of the feedback laws in the examples of this paper can be said in general to be a help or a hindrance to the robust performance. However, it seems likely that existing techniques from robust nonlinear control theory could be employed to answer these questions.

Acknowledgments

The authors gratefully acknowledge support for this research through NSF grant CMMI-0747563. The views expressed in this paper are those of the authors, and do not necessarily reflect those of the National Science Foundation.

References

[1] S. Roundy, P.K. Wright, J. Rabaey, A study of low level vibrations as a power source for wireless sensor nodes, *Journal of Computer Communications* 26 (2002) 1131–1144.

[2] C. Knight, J. Davidson, S. Behrens, Energy options for wireless sensor nodes, *Sensors* 8 (2008) 8037–8066.
[3] H.A. Sodano, D.J. Inman, G. Park, Comparison of piezoelectric energy harvesting devices for recharging batteries, *Journal of Intelligent Material Systems and Structures* 16 (2005) 799–807.
[4] Y.C. Shu, I.C. Lien, Analysis of power output for piezoelectric energy harvesting systems, *Smart Materials and Structures* 15 (2006) 1499–1512.
[5] L. Zuo, B. Scully, J. Shestani, Y. Zhou, Design and characterization of an electromagnetic energy harvester for vehicle suspensions, *Smart Materials and Structures*19 (2010) #045003.
[6] C. Nagode, M. Ahmadian, S. Taheri, Effective energy harvesting devices for railroad applications, *Proceedings of the SPIE Conference on Smart Structures/NDE*, Vol. 7643, San Diego, CA, 2010.
[7] S.M. Lattanzio, J.T. Scruggs, Maximum power generation of a wave energy converter in a stochastic environment, *Proceedings of the IEEE International Conference on Control Applications*, Denver, CO, 2011, pp. 1125–1130.
[8] T. Ni, L. Zuo, A. Kareem, Assessment of energy potential and vibration mitigation of regenerative tuned mass dampers on wind excited tall buildings, *Proceedings of the ASME International Design Engineering Technical Conferences*, Washington, DC, 2011.
[9] G.K. Ottman, H.F. Hofmann, G.A. Lesieutre, Optimized piezoelectric energy harvesting circuit using step-down converter in discontinuous conduction mode, *IEEE Transactions on Power Electronics* 18 (2003) 696–703.
[10] E. Lefeuvre, D. Audigier, C. Richard, D. Guyomar, Buck-boost converter for sensorless power optimization of piezoelectric energy harvester, *IEEE Transactions on Power Electronics* 22 (2007) 2018–2025.
[11] T. Paing, J. Shin, R. Zane, Z. Popovic, Resistor emulation approach to low-power RF energy harvesting, *IEEE Transactions on Power Electronics* 23 (2008) 1494–1501.
[12] N. Kong, D.S. Ha, A. Erturk, D.J. Inman, Resistive impedance matching circuit for piezoelectric energy harvesting, *Journal of Intelligent Material Systems and Structures* 21 (2010) 1293–1302.
[13] J.T. Scruggs, An optimal stochastic control theory for distributed energy harvesting networks, *Journal of Sound and Vibration* 320 (2009) 707–725.
[14] J.T. Scruggs, On the causal power generation limit for a vibratory energy harvester in broadband stochastic response, *Journal of Intelligent Material Systems and Structures* 21 (2010) 1249–1262.
[15] I.L. Cassidy, J.T. Scruggs, S. Behrens, Optimization of partial-state feedback for vibratory energy harvesters subjected to broadband stochastic disturbances, *Smart Materials and Structures*20 (2011) #085019.
[16] D.L. Margolis, The response of active and semi-active suspensions to realistic feedback signals, *Vehicle System Dynamics* 11 (1982) 267–282.
[17] D. Karnopp, Active damping in road vehicle suspension systems, *Vehicle System Dynamics* 12 (1983) 291–311.
[18] D. Horvat, Survey of advanced suspension developments and related optimal control applications, *Automatica* 33 (1997) 1781–1817.
[19] G.W. Housner, L.A. Bergman, T.K. Caughey, A.G. Chassiakos, R.O. Claus, S.F. Masri, R.E. Skelton, T.T. Soong, B.F. Spencer, J.T.P. Yao, Structural control: *past, present, and future*, *Journal of Engineering Mechanics* 123 (1997) 897–971.
[20] M.D. Symans, M.C. Constantinou, Semi-active control systems for seismic protection of structures: *a state-of-the-art review*, *Engineering Structures* 21 (1999) 469–487.
[21] S.J. Dyke, B.F. Spencer, M.K. Sain, J.D. Carlson, Modeling and control of magnetorheological dampers for seismic response reduction, *Smart Materials and Structures* 5 (1996) 565–575.
[22] Z.G. Ying, W.Q. Zhu, T.T. Soong, A stochastic optimal semi-active control strategy for ER/MR dampers, *Journal of Sound and Vibration* 259 (2003) 45–62.
[23] H.E. Tseng, J.K. Hedrick, Semi-active control laws—optimal and sub-optimal, *Vehicle System Dynamics* 23 (1994) 545–569.
[24] J.T. Scruggs, A.A. Taflanidis, W.D. Iwan, Non-linear stochastic controllers for semiactive and regenerative systems with guaranteed quadratic performance bounds—part 1: *state feedback control*, *Structural Control and Health Monitoring* 14 (2007) 1101–1120.
[25] J.T. Scruggs, Multi-objective nonlinear control of semiactive and regenerative systems, *Proceedings of the American Control Conference*, Baltimore, MD, 2010, pp. 726–731.
[26] J.T. Scruggs, Structural Control Using Regenerative Force Actuation Networks, Ph.D. Thesis, California Institute of Technology (2004).
[27] R. Lozano-Leal, S. Joshi, On the design of dissipative LQG-type controller, *Proceedings of the IEEE Conference on Decision and Control*, Austin, TX, 1988, pp. 1645–1646.
[28] R.W. Erickson, *Fundamentals of Power Electronics*, Chapman and Hall, 1997.
[29] P. Dorato, C.T. Abdallah, V. Cerone, *Linear-Quadratic Control*, Prentice-Hall, 1995.
[30] J.T. Scruggs, W.D. Iwan, Optimal nonlocal and asymmetric structural damping using regenerative force actuation networks, *Journal of Engineering Mechanics* 132 (2006) 932–940.
[31] K.J. Åström, *Introduction to Stochastic Control Theory*, Dover, 1970.
[32] I.L. Cassidy, J.T. Scruggs, S. Behrens, H.P. Gavin, Design and experimental characterization of an electromagnetic transducer for large-scale vibratory energy harvesting applications, *Journal of Intelligent Material Systems and Structures* 22 (2011) 2009–2024.
[33] H.A. Sodano, G. Park, D.J. Inman, Estimation of electric charge output for piezoelectric energy harvesting, *Strain* 40 (2004) 49–58.
[34] J.K. Hedrick, R. Rajamani, K. Yi, Observer design for electronic suspension applications, *Vehicle System Dynamics* 23 (1994) 413–440.
[35] J.T. Scruggs, A.A. Taflanidis, W.D. Iwan, Non-linear stochastic controllers for semiactive and regenerative systems with guaranteed quadratic performance bounds—part 2: *output feedback control*, *Structural Control and Health Monitoring* 14 (2007) 1121–1137.